On steady homogeneous sand–water flows in a vertical conduit

F. GALLO and A. W. WOODS
BP Institute, University of Cambridge, Madingley Rise, Madingley Road, Cambridge CB3 0EZ, UK
(E-mail: federico@bpi.cam.ac.uk)

ABSTRACT

In this paper, an idealized model of the steady-state phase of the flow in a vertical conduit leading to a sand volcano eruption is developed from first principles. The model assumes that a sand–water mixture flows upwards, driven by an overpressure at the base of a vertical cylindrical conduit (or a two-dimensional fracture) and opposed by gravity, viscous resistance and turbulent drag. The conditions for flow are analysed in detail, and the mechanisms controlling the eruption rates are studied quantitatively. The flow predictions are in accordance with our observations of analogous vigorous sand eruptions at deepwater oil fields. For sufficiently high flow velocities ($u > 10u_T$) and small sand fractions ($s < 0.2$), the flow may be well mixed and homogeneous. If these conditions are not met, the flow may either become two phase or does not develop. Combining geological considerations with the steady homogeneous model, it is possible to predict the behaviour of the vigorous quasi-steady stage of a sand volcano eruption. It is shown that, based on the average density of the overlying sediments, there are a range of overpressures for which sand volcanoes may develop.

Keywords Sand volcanoes, sandstone dykes (dikes), sandstone intrusions.

INTRODUCTION

Sand injections have been identified around the world for over a century (e.g. Diller, 1889; Cross, 1893; Newson, 1903), in sites such as Tierra del Fuego, Argentina (Borrello, 1962), California (Newson, 1903) and South Africa (Truswell, 1972). They are manifest in the form of both sand intrusions, such as dikes and sills (Waterson, 1950; Winslow, 1983; Huang, 1988), and sand extrusions, such as sand volcanoes and boils (Housner, 1958; Obermeier, 1996, 1998; Galli, 2000; Takahama *et al.*, 2000). At many sites, both sand intrusions and extrusions can be clearly observed (Gill & Kuenen, 1957; Boehm & Moore, 2002; Strachan, 2002), which implies that the two phenomena are closely related. Some recently studied examples of sand intrusions occur deep underwater in the Alba and Harding hydrocarbon reservoirs in the North Sea, where sand injections significantly impact on both reservoir development and production (Lonergan *et al.*, 2000). The Bruce-Baryl Embayment (Dixon *et al.*, 1995) represents another offshore case.

All the above cases occurred spontaneously in nature. Most descriptions of sand injections are associated with sedimentary layers, although some have been documented to penetrate igneous layers (Cross, 1893). There are also cases where sand volcanoes have been induced by human activity (Neumann-Mahlkau 1976). For example, sand extrusions may be triggered by the submarine drilling of boreholes; this phenomenon is known in the hydrocarbon industry as shallow water flow (Alberty *et al.*, 1997).

This wide variety of distinct and apparently unrelated phenomena can be traced back to a common origin: the generation of porewater overpressure in the source bed, which causes the sand remobilization. In a review of published literature, Jolly & Lonergan (2002) suggest that there may be four triggering mechanisms capable of generating an elevated pore pressure and hence triggering a sand injection: (1) seismically induced liquefaction; (2) tectonic stress; (3) localized excess pore fluid pressures generated by depositional related processes; and (4) the influx of an overpressured fluid from

deeper within the basin into a shallow sand body.

Sand injections are believed to be a relatively common process following the deposition of uncemented, water-saturated sand (source bed) rapidly sealed by a semi-impermeable mud layer (host bed). During the early stages of burial and diagenesis, the formation of hydraulic fractures, later filled by sands from the underlying source, is thought to be an important factor in the movement of fluids through and out of the low-permeability, overlying sediments, which may or may not be lithified (Cosgrove, 2001).

One hypothesis for the formation of sand intrusions suggests that injections into the host bed occur when the fluid pressure in the pores exceeds the strength of the overlying sediments. The overpressure therefore opens a conduit, a planar fracture or a cylindrical pipe, and forces a fluidized sand–water mixture to be injected (Cosgrove, 2001). When sand injections propagate upwards, in the direction of decreasing lithostatic pressure, the sand-filled conduits may intersect the surface, or the seabed, in which case they can give rise to sand volcanoes (Obermeier, 1996, 1998).

The literature shows that a great deal of work has been directed to the description and classification of many field examples observed around the world. The complexity of these phenomena is made evident by the wide range of scales and types of sand injections reported. Many reports provide a qualitative interpretation of the observations. In particular, the mechanisms controlling the seismic triggering of the pore overpressure in shallow sediments are being investigated in growing detail. The knowledge gained is also used to address related problems. For example, the remains of sand volcanoes that are believed to have been triggered by seismic activity are being used in the field of palaeoseismicity (Obermeier, 1996; 1998). However, this topic is a poorly understood area of research. There are relatively few qualitative studies of the fundamental dynamics of these processes. Typically, the analysis is restricted to the specific site under study. Some quantitative studies have been proposed; for example Housner (1958) considered the case of seismically induced sand blows when the low-permeability, overlying seal is not present above the source bed.

The goal of this paper is to begin to identify and quantify some of the fundamental physical processes involved in the general dynamics of sand injections. This work represents one step as part of a longer term project that aims to understand sand injections as a whole. From the point of view of this framework, sand volcanoes, sandstone dikes and sills as well as shallow water flows are particular manifestations of a more general underlying process, with the different phenomena arising when different boundary conditions are met.

In this paper, the control of the properties of the overlying, low-permeability host bed on the geometry of the sand injections is outlined. Once the general picture has been presented, attention is focused on cylindrically shaped conduits, which represent the characteristic geometry at shallow depths. These can intersect the surface and lead to sand volcanoes. The flow within this conduit will be described with a homogeneous, steady physical model, and the limiting assumptions will be carefully justified. The constraints on the model will then be quantified and the results derived presented in detail. The relevance of the model to observed sand volcanoes is then discussed. Flow predictions are compared with data obtained from analogous processes observed in deep offshore wells during drilling. Finally, the model is adapted to the planar geometry of sandstone dikes, and its validity in this domain is discussed.

CONDUIT GEOMETRY AND FLOW REGIMES

Sand injections can manifest themselves in many geometries and sizes even though they are all created by the release of the pore fluid overpressure in the source bed. The reason why sand injections are so varied is that the geometry of clastic intrusions is controlled by the mechanical behaviour of the sedimentary layers in which the fluidized sand is injected, the host bed.

Cylindrical pipes

Experiments show that intrusions into loose sand result in cylindrical conduits with splayed ends, whereas injections into clay-rich unconsolidated sediment lead to the formation of smaller pipes (Nichols *et al.*, 1994; Nichols, 1995). This is confirmed by the fact that, in a large number of geological field reports, sand injections are reported as intersecting the surface and creating small conic craters, the centres of which coincide with

the vertical pipe (e.g. Gill & Kuenen, 1957; Obermeier, 1996).

Reports on cylindrical pipes suggest that their depths range between 0·5 m and 20 m (Seed, 1979; Walsh *et al.*, 1995; Obermeier, 1996). The diameter of the conduit is usually less than 0·5 m but, in exceptional cases, it can be as large as 1·5 m (Gill & Kuenen, 1957). If the conduit intersects the surface, a cone of extruded sand will be created with a crater at the centre. Field observations suggest that the diameter of such craters may be as large as one-third that of the cone. The slope of the cone is usually smooth and at an angle of 10–15°, which suggests low sand concentrations in the upward-flowing water (Gill & Kuenen, 1957).

Planar dikes

If the sediments have undergone partial lithification so that there are cohesive forces holding the grains together, high water pressures in the source bed will cause the overlying rock to fracture according to the stress state of the basin. Field observations show that two types of dikes occur in nature: (1) vertical dikes; and (2) diagonal dikes. Figure 1 shows an example of a vertical dike observed by the Ewan River in Tierra del Fuego, Argentina. Figure 2 shows an example of a shear fracture that was injected with sand; the diagonal dike was observed at Cabo San Pablo in Tierra del Fuego, Argentina. Apart from the thick dike extending from the bottom left to the top right of the picture, thinner dikes can be seen rising in both the same and opposite directions, as originally documented by Borrello (1962).

Sand intrusions are thought to form generally within sedimentary successions at burial depths of less than about 1000 m. A peculiar example occurs in Tierra del Fuego, where the source beds of the clastic intrusions underlie a shale 1400 m thick. Sandstone dikes range in thickness from a thin film to tens of metres, in a couple of extreme cases reaching a width of almost 250 m (Cross, 1893). In plan view, their lengths can vary from a few centimetres to 10 km: the Great Dike in northern California runs for about 15 km (Diller, 1889). The material transported by the flow is usually composed of well-sorted, pure sand with grains of 0·5–1 mm in diameter. But, in some cases, it may be made up of chaotic, poorly sorted, volcanoclastic sandstone with clasts up to 0·25 m in diameter (Winslow, 1983).

Generally, pipe-shaped conduits may be expected to form close to the surface, where sediments

Fig. 1. Vertical dike. Ewan River in Tierra del Fuego, Argentina.

Fig. 2. Diagonal dike. Cape San Pablo, Tierra del Fuego, Argentina.

tend not to be consolidated. Planar dikes, on the other hand, are expected to occur at greater depths, where the overlying weight causes the deposits to lithify. Often dikes make complex three-dimensional geometries. This may be caused either by the intersection of shear fractures or by a more complex stress state in the host bed than assumed above.

Flow regimes

The observations suggest that the dynamics of a natural sand intrusion flow may be divided into a series of qualitatively different stages. First, there is the upward propagation of a conduit into the overlying sediments. This may be either a planar fracture or a cylindrical channel, depending on the behaviour of the host sediments. The latter may intersect the surface; if this happens, a second quasi-steady, flowing stage may develop in which a sand–water mixture is continuously extruded into the environment. In many cases, the volume of the cone-shaped structures is relatively large compared with the size of the conduits that produced them. Also, the cones tend to be symmetrical and smooth. This suggests that the flow may have been dilute and relatively long-lived compared with the time to erupt the volume of the sand–water mixture in the conduit. There are examples, on the other hand, where this criterion suggests that the quasi-steady stage may have been very short-lived or absent altogether. The final stage is determined by the rundown: as the source is depleted and the porewater overpressure is dissipated, the conduit shuts down, clogs up and the upward flow comes to rest. In the analogue processes produced by the artificial drilling of boreholes, the first stage is obviously absent, while the quasi-steady stage has been systematically observed in different well bores since 1985 (Alberty, 2000).

If the quasi-steady stage takes place, three distinct flow regimes may be envisaged. At high velocities and low sand concentrations, the interaction between sand grains is negligible: the flow may be considered to be well mixed and homogeneous. At sand concentrations higher than 20%, grain–grain interactions are important, and the flow becomes two-phase. Finally, for low velocities, the water flow is not able to carry the sand grains upwards, and the system behaves as a single-phase flow through the permeable sand layer left after the extrusion stage has terminated.

The complexity of the processes involved in sand injections makes the study of these phenomena a formidable task. Because of this, the present work aims generally to provide a framework focusing on an idealized, homogeneous, sand–water flow during the quasi-steady regime in a vertical, cylindrical conduit, which is amenable to quantitative analysis. As well as quantifying the process, one key output of the model is the recognition of the conditions under which the model ceases to apply and other regimes develop.

THE PHYSICAL MODEL

Qualitative description

In this section, a model of the intermediate quasi-steady flow of a sand–water mixture up a cylindrical conduit from the subsurface is developed. The model is used to provide insight into the physics of the system and to determine conditions necessary for a vigorous sand–water flow in a geological context, and it is compared with observations from submarine drilling operations. The controls on the flow rates during the quasi-steady phase are studied, focusing on the sand–water ratio of the erupting mixture, the conduit geometry and the overpressure relative to the hydrostatic pressure in the basin. Other important controls are the height H and radius r of the conduit.

The model assumes that a cylindrical conduit is created during the initial upward propagation phase. The sand–water flow is assumed to be steady, homogeneous and well mixed, and is described by averaged quantities appropriate for a vigorous flow. It is important to bear in mind that these conditions are consistent with, and apply only to, the specific flow regime under study, as outlined above. The model predictions are then used to determine when this assumption is consistent with the actual flow regime, and hence to determine the range of subsurface conditions necessary to produce such a flow.

The quantitative model

A sand–water mixture, with average density ρ and effective viscosity μ flows upwards with mean velocity u in the positive z direction driven by an overpressure Δp at the base of a cylindrical conduit of height H and diameter $2r$ (Fig. 3). The overpressure at the base of the conduit, Δp, drives the flow upwards through the conduit. The overpressure is defined as $\Delta p = p(0) - \rho_W g H$, where $p(0)$ is the pressure at the bottom of the conduit ($z = 0$), and $\rho_W g H$ is the hydrostatic pressure at ($z = 0$). The properties of the mixture, such as viscosity μ and density ρ, are assumed to take averaged values across the conduit and depend on the concentration of sand in the flowing water; this is in accordance with the homogeneous flow assumption.

The motion of the fluid is governed by the equations of conservation of momentum and mass for the mixture. The present analysis makes
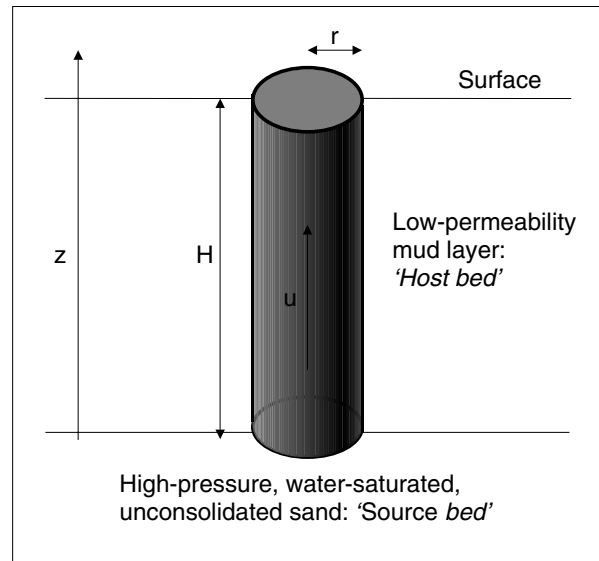

Fig. 3. Diagram of the idealized upward flow through a cylindrical conduit.

use of the homogeneous flow model, which is based on the assumptions that flow is steady, well mixed and in equilibrium, as discussed above. For other flow rates, the motion becomes two-phase and unsteady with slip between the fluid and solid particles, but this goes beyond the scope of this paper.

In the model, no mass is lost from the conduit, and therefore the conservation of mass in the ascending flow has the form:

$$\frac{dQ_W}{dz} = \frac{dQ_S}{dz} = 0 \tag{1}$$

where Q_W and Q_S are the volumetric water and sand fluxes, respectively, and they are measured in m^3 s^{-1}. The equation implies that the flow velocity is constant throughout the conduit. It follows from the principle of conservation of momentum that the pressure gradient must be balanced by gravitational and frictional forces:

$$\frac{dp}{dz} = -\rho g - \frac{8\mu u}{r^2} - \frac{\rho C_D u^2}{r} \tag{2}$$

where $-\frac{8\mu u}{r^2}$ and $-\frac{\rho C_D u^2}{r}$ represent the viscous and turbulent drag, respectively, which together constitute the frictional resistance to motion (Wallis, 1969). In Eq. (2), ρ is the average density; $p(z)$ the pressure; g the acceleration of gravity; s the sand content; $\mu(s)$ the effective viscosity, which

depends on the sand fraction; and $C_D \approx 10^{-2}$ is the coefficient of friction, an empirical quantity that has been tabulated by Moody (1944) and depends on the roughness of the walls.

The equations are combined with relationships between the average velocity, the average density, the viscosity and the sand fraction. The sand volume fraction is given by the volume of sand divided by the total volume:

$$s = \frac{Q_S}{Q_S + Q_W} \qquad (3)$$

The average density is then simply given by:

$$\rho = s\rho_S + (1 - s)\rho_W \qquad (4)$$

where ρ_W and ρ_S are the densities of water and sand respectively.

The average velocity is defined as the total volumetric flow divided by the cross-sectional area of the conduit: $u = \frac{Q_S + Q_W}{\pi r^2}$. Equation 4 allows the average velocity to be expressed in terms of the sand volume fraction:

$$\rho w u = \rho_S Q_S + \rho_W Q_W \qquad (5)$$

The above system of equations is complete once the relation between sand content and viscosity has been specified. By comparison with experiments, the effects may be parameterized by an empirical relationship of the form:

$$\mu(s) = \mu_0 \left(1 - \frac{s}{s_C}\right)^{-\frac{5}{2}} \qquad (6)$$

where μ_0 is the viscosity of pure water, and $s_C = 0\cdot74$ (Marsh, 1981). As the sand fraction is increased, the key point to note is that the mixture exerts more resistance to motion and, eventually, the grains will be in contact with one another, and the mixture ceases to flow when $s \sim s_C = 0\cdot74$. This depends on the shape and distribution of the grains, but a representative value used in these calculations is $s_C = 0\cdot74$. At this point, there is a solid, porous matrix that effectively applies an infinite resistance to the flow. Alternative parameterizations with the same general character also exist (Wallis, 1969). The main differences between these expressions arise at high sand concentrations as the particles become close packed and approach the threshold of no flow. However, for smaller sand fractions Eq. (6) provides a satisfactory parameterization of the data consistent with the assumption of small

sand concentrations, i.e. $s < 0\cdot2$, which is in accordance with the homogeneous flow assumption.

Finally, one boundary condition is needed for the system to be fully determined. This is achieved by fixing the pressure at the top of the conduit, $p(H) = p_T$. In order to simplify the mathematical analysis, it is useful to set $p_T = 0$. This does not affect the nature of the results, which only depend on the pressure difference between the top and the bottom of the conduit. This implies that, as far as the pressure is concerned, there is no difference whether the mixture is being extruded deep under water on the seabed or in a subaerial setting. The only necessary requirement is that p_T equals the outside ambient pressure. The real pressure $P(z)$ can then be easily obtained by adding p_T to the pressure in the conduit, i.e. $P(z) = p(z) + p_T$.

The exact flow rates are determined by the overpressure at the bottom of the conduit, $\Delta p = p(0) - \rho_W g H$, which is defined relative to the hydrostatic pressure; the sand load carried by the flow, s; as well as by the geometry of the conduit, described by the height H and the radius r.

PREDICTIONS OF THE MODEL

In this section, the flow rates predicted by the homogeneous flow model are presented, and the sensitivity of these results to sand concentration, conduit geometry and initial overpressure is explored.

Combining Eq. (2) with the boundary condition that $p(H) = p_T = 0$, it is found that:

$$p(z) = \left(\rho g + \frac{8\mu u}{r^2} + \frac{\rho C_D u^2}{r}\right)(H - z) \qquad (7)$$

This equation implies that the pressure $p(z)$ decreases linearly with height z. At $z = H$, the pressure becomes $p = 0$, as required by the boundary condition. As mentioned above, the flow velocity is determined by the overpressure Δp at $z = 0$. With the aid of Eq. (4), a relationship between Δp, the velocity u and the sand fraction s may be found:

$$\frac{\Delta p}{H} = s(\rho_S - \rho_W)g + \frac{8\mu u}{r^2} + \frac{\rho C_D u^2}{r} \qquad (8)$$

This has two roots for u and, for upward flow $(u > 0)$, the positive one is chosen:

$$u = -\alpha + \sqrt{\alpha^2 + \gamma} \qquad (9)$$

where $\alpha = \frac{4\mu}{\rho C_D r}$ represents the velocity for which the viscosity and the turbulent drag are comparable, and $\sqrt{\gamma} = \sqrt{\frac{r}{\rho C_D}\left((\rho_W - \rho_S)sg + \frac{\Delta_p}{H}\right)}$ denotes the flow speed in which the overpressure is balanced by the turbulent resistance alone.

Figures 4–8 illustrate some typical flow rates as a function of the key controlling parameters. In all the figures, the following parameter values are taken, unless specified otherwise: $H = 3$ m, $r = 0.01$ m, $\rho_W = 1000$ kg m^{-3}, $\rho^S = 2650$ kg m^{-3}, $\Delta p = (\rho_L - \rho_W)gH = 14\,700$ Pa, which represents the maximum possible overpressure, as will be explained below. ρ_L represents the bulk density of the overlying sediment and will be used in later sections. An estimate of the value is difficult to obtain because it depends on the porosity of the sediment, which in turn varies with depth. Here, an average value $\rho_L = 1500$ kg m^{-3} is assumed.

Figure 4 shows the velocity u as a function of sand fraction s. For low sand contents, the turbulent drag associated with the flow balances the overpressure. However, for high values of s, i.e. $s > 0.2$, the collisions between grains become increasingly important and cause clusters of grains to start forming, making the flow unsteady and non-homogeneous. At even higher sand concentrations, the collisions between grains alter the average properties of the mixture, which now opposes a higher resistance to the flow. In this domain, the effective viscosity μ grows abruptly and becomes dominant. These, however, lie beyond the homogeneous flow regime. The graph also shows that, as the radius, r, is increased, so is the velocity. This is because the flow is fastest at the centre of the conduit, but is retarded by friction against the walls. The smaller the radius, the bigger the total frictional effect that the walls exert upon the fluid. This is evident from the turbulent and viscous drag terms in Eq. (2), where a reduction
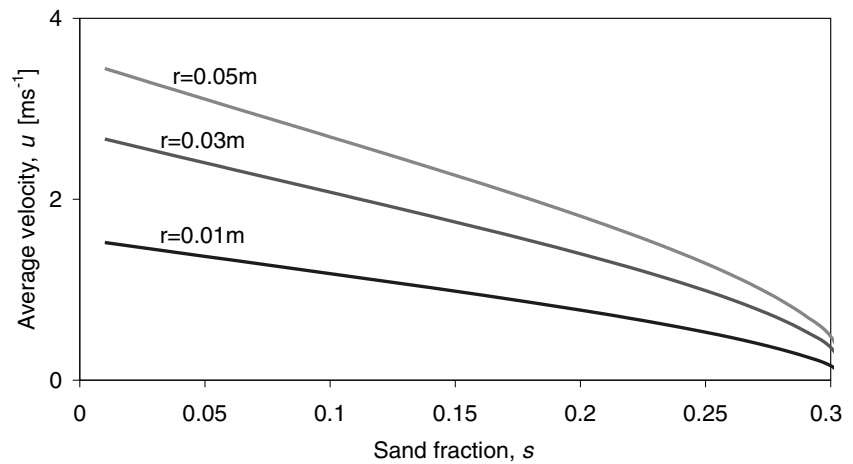

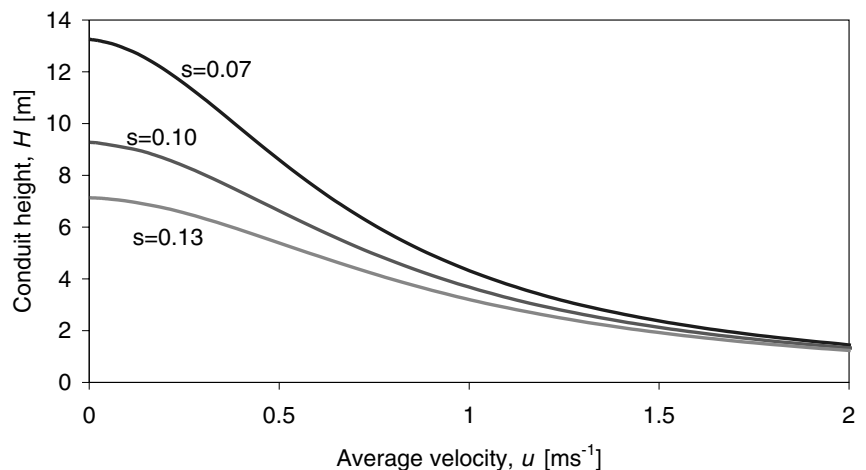**Fig. 4.** Velocity u as a function of sand fraction s.

Fig. 5. Velocity u as a function of conduit height H for a given overpressure Δp.

in r in the denominator causes the friction to increase.

Figure 5 shows how the velocity u varies as a function of conduit height H for a given overpressure Δp. As H is increased, the flow speed decreases; this is for two reasons. First, more work is required to move a given mass of sediment along a greater distance against the pull of gravity. Secondly, for longer conduits, more work has to be done against the turbulent and viscous drags.

Figure 6 shows the velocity u as a function of the conduit radius r for a given overpressure at the bottom of the fracture, Δp. This diagram is useful to understand the delicate balance between the turbulent and viscous resistance to motion. The non-linearity of the curves clearly shows that the flows are dominated by turbulence; this can be traced back to the fact that the turbulence term is proportional to u^2. For a small radius, the viscous effects are augmented by the closeness of the walls. However, the graph shows that, except for the thinnest conduits, i.e. $r < 0.002$ m, where the curves become concave upwards signifying that the curve turns linear, the viscous term is negligible. This fact can be seen better by defining the drag ratio: $D_R = \frac{turbulent\ drag}{viscous\ drag} = \frac{\rho C_D \bar{u} r}{8\mu}$. If $D_R > 1$, the turbulence drag is dominant; whereas, for $D_R < 1$, the viscous drag becomes dominant. Figure 7 shows that, for the various sand fractions consistent with the homogeneous flow assumption, the viscous drag is negligible unless the diameter of the conduit is of the order of the size of the sand grains. In this range, however, the model loses physical meaning. It is therefore a necessary conclusion that, in the homogeneous flow regime, the dominant frictional term is provided by the turbulent drag. As the radius is increased, the flow is free to accelerate until the velocity is high enough for the turbulent forces to intervene and oppose the motion.
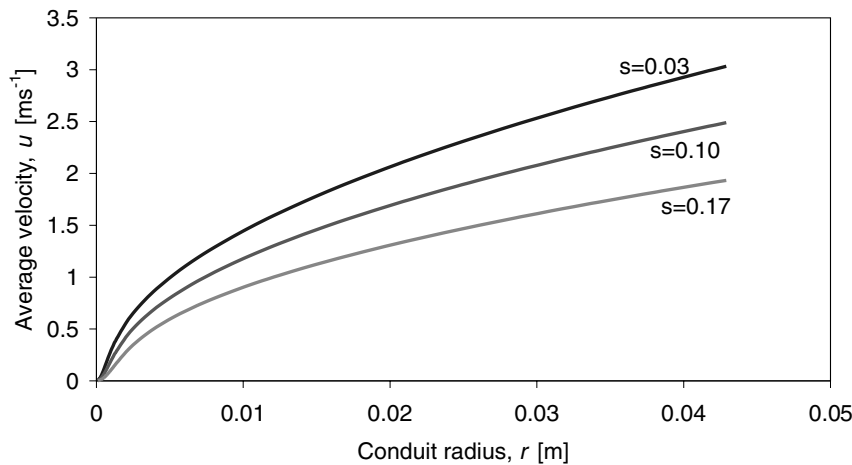

Fig. 6. Velocity u as a function of conduit width w for a given overpressure at the bottom of the fracture Δp.
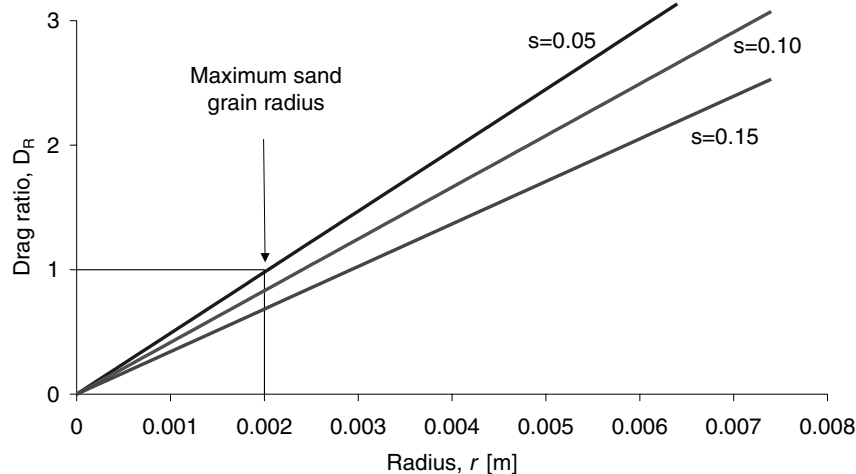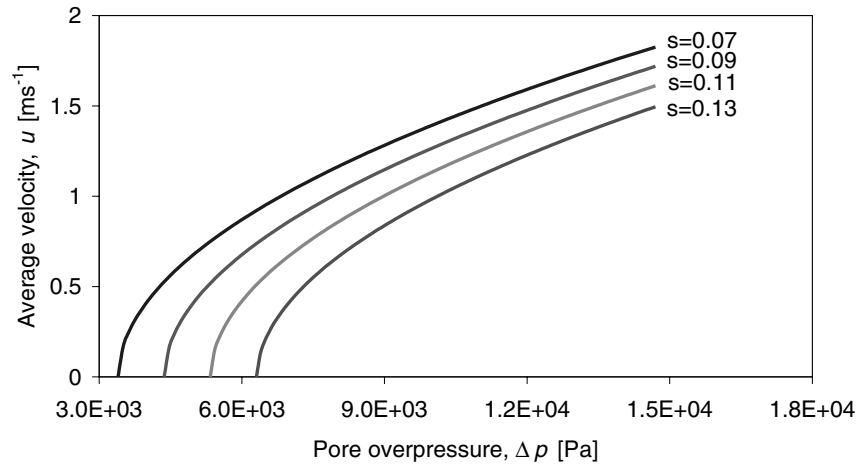

Fig. 7. The turbulent drag is dominant unless the radius of the conduit is in the order of the grain size.

Fig. 8. Average velocity *u* as a function of overpressure Δp for several values of the sand fraction *s*.

Figure 8 shows the average velocity *u* as a function of overpressure Δp for several values of the sand fraction *s*; it also illustrates the effects of gravity and turbulence. For large *s*, the average density increases, and the weight of the column is greater: a higher fraction of Δp is required to balance this increase, and so the effective overpressure available to drive the flow is smaller. If $\Delta p < s(\rho_S - \rho_W)gH$, there is insufficient overpressure to drive a flow. If Δp is high enough to balance the weight of the column and drive the flow upwards, the turbulent drag determines the velocity at which the mixture will flow upwards, and this will be at a rate proportional to $\sqrt{\Delta p} - s(\rho_s - \rho_w)gH$.

In summary, the flow is driven upwards by the excess pore pressure, defined as $\Delta p = p(0) - \rho_W gH$. The overpressure is dissipated throughout the conduit by doing work against the action of gravity and friction, which oppose the flow. A fraction of the overpressure $\Delta p_g = s(\rho_S - \rho_W)gH$ supports the weight of the sand mixture in the fluid. The remaining overpressure, $\Delta p_v = \Delta p - s(\rho_S - \rho_W)gH$, drives the flow. This is opposed by the frictional force, which is a combination of the viscous, $\frac{12\mu u H}{w^2}$, and the turbulent, $\frac{\rho C_D u^2 H}{w}$, terms. In the homogeneous regime, which is characterized by low sand concentration, the turbulent drag is the dominant frictional factor.

An increase in *H* slows down the flow because it both affects the total weight of the column and prolongs the pressure dissipation against friction. If the radius of the conduit, *r*, is decreased, the flow will also slow down because of the increased friction effects due to the walls of the conduit. Finally, the sand fraction *s* affects both the weight of the column, through its impact on the average density (Eq. 4), and the effective viscosity of the mixture, which does not, however, have a

significant impact on the dynamics of the system at low sand concentrations.

CONSTRAINTS ON THE VALIDITY OF THE PHYSICAL MODEL

The model developed for the sand–water flow in an open vertical conduit is based on the assumption of homogeneous and steady flow. Here, conditions consistent with these assumptions are analysed, in particular taking into account the geological constraints on the magnitude of the overpressure Δp as a function of the height *H* of the conduit. Sand volcanoes and, more generally, sand injections will occur only if certain conditions are met. The maximum pore overpressure Δp_{MAX} in the basin is determined by the weight of the overlying rock or sediment making up the low-permeability layer. The speed of the flow is given in terms of the overpressure $\Delta p < \Delta p_{MAX}$ according to Eq. (9), as long as the condition for homogeneous flow is satisfied. This requires that the average velocity is large compared with the terminal fall speed u_T of the individual sand grains; otherwise, the flow becomes two-phase and unsteady. These conditions will now be quantified and discussed in detail.

Constraints on the overpressure at depth

The geometry of the system imposes an upper limit on the overpressure. The pore pressure deviates from hydrostatic because of the weight of the overlying sediments. As a simple model, a homogeneous bulk density of the overlying sediment, ρ_L, is assumed. The maximum overpressure is then a function of the conduit height *H*:

$$\Delta P_{MAX} = (\rho_L - \rho_W)gH \qquad (10)$$

Conditions for homogeneous flow

The mixture moves upwards as a homogeneous fluid only if the mean speed is much greater than the fall speed of the grains. If this condition is not met, the flow ceases to be well mixed, localized clusters of particles form and the flow becomes two-phase. As the sand grains are denser than water, they will flow with lower upward velocity than the water, according to:

$$u_S = u_W - u_T \qquad (11)$$

where u_W is the water velocity and u_T is the terminal velocity of the sand grains. There are a number of empirical relations based on experimental data that parameterize the fall speed as a function of Reynolds' number. Here, the well-known Stoke's law, valid for spherical particles, is adapted for all Reynolds' numbers. The radius of the spherical particles is interpreted as one half the mean grain radius:

$$u_T = \sqrt{\frac{4}{3}\frac{d}{C_F}\frac{\rho_S - \rho_W}{\rho_W}g} \qquad (12)$$

where $C_F = \frac{24}{Re}(1 + 0.15Re^{0.687})$ for Re < 1000 and $C_F = 0\cdot44$ for Re > 1000, with Re $= \frac{u_T d\rho_W}{\mu_0}$ being the Reynolds number for the flow and d the particle diameter (Wallis, 1969). The fall speeds are found by solving the implicit relation (12), and they are shown in Fig. 9 as a function of diameter d.

It is important to note that Eq. (12) is only valid for unhindered settling, which takes place when the grain–grain interactions are negligible. As this paper is only concerned with low-concentration flows, Eq. (12) is an acceptable approximation.
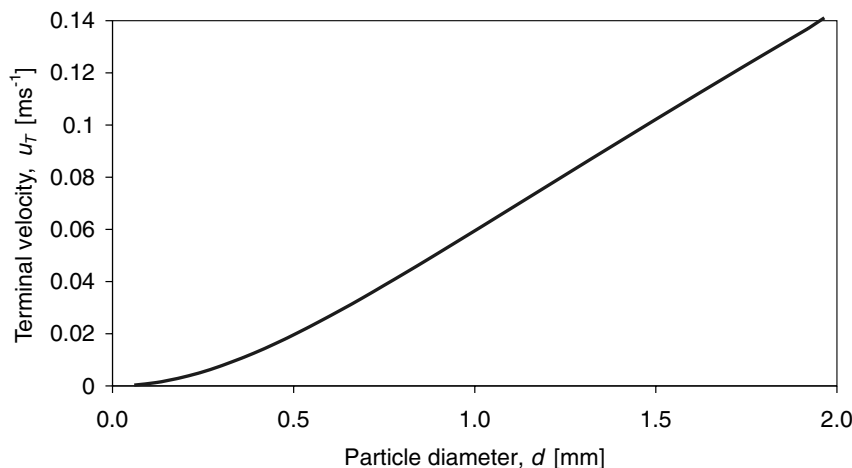
The average velocity u is related to u_W and u_S by:

$$u = su_S + (1 - s)u_W \qquad (13)$$

Combining this with Eq. (11), the relationship $u = u_W - su_T$ is obtained. For the flow to be well mixed and homogeneous, the velocities of water and sand have to be comparable; otherwise, owing to slip effects between the sand particles and water, the mixture will become two-phase and the flow would become unsteady. The flow will be homogeneous when $u_W \gg u_T$, so $u \sim u_W$. As a simple criterion, the condition that $u > u_{T'} = 10u_T$, is used to delineate homogeneous flow. The threshold overpressure Δp_{UT}, above which the mixture can safely be considered to be well mixed, may be found by substituting $u_{T'}$ into Eq. (8):
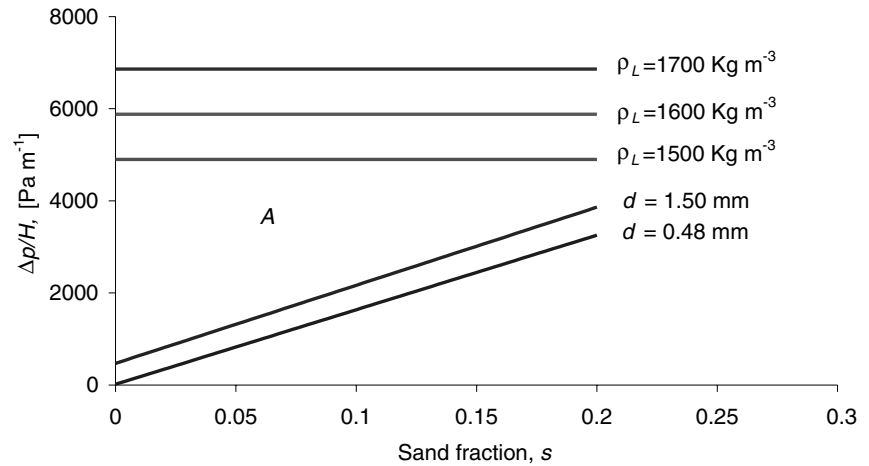
$$\Delta p_{UT} = \left(\frac{8u'_T\mu}{r^2} + \frac{u'^2_T\rho C_D}{r} + (\rho_s - \rho_w)sg\right)H \qquad (14)$$

Taking the above physical constraints, and assuming that a conduit exists, it can be safely maintained that the present model applies for overpressures in the range $\Delta p_{UT} < \Delta p < \Delta p_{MAX}$. Under these conditions, a homogeneous, quasi-steady flow of sand and water may develop at a rate described by Eq. (9) and governed by the mechanisms outlined earlier. Figure 10 illustrates the region where the homogeneous flow assumption is expected to be valid. The graph shows the

Fig. 9. Terminal velocity u_T as a function of particle diameter d.

Fig. 10. Homogeneous flow occurs in region A, which is bounded at the top by the maximum overpressure, $\Delta p_{MAX}(\rho_L)$, and at the bottom by the homogeneous flow condition, $\Delta p_{UT}(d)$. These, in turn, are determined by the average density of the sediments, ρ_L, and the diameter of the sand grains, d, respectively.

pressure drop per unit height, $\Delta p/H$, as a function of sand fraction, s. $\Delta p_{MAX}/H$ is independent of s, hence a constant in the graph; three values are shown for $\rho_L = 1700$ kg m^{-3}, $\rho_L = 1600$ kg m^{-3} and $\rho_L = 1500$ kg m^{-3}. On the other hand, $\Delta p_{UT}/H$ is dependent upon s, and a function of the diameter of the grains. The two lines for $\Delta p_{UT}/H$ are examples where $d = 0.48$ mm and $d = 1.50$ mm, leading to $u_T = 0.018209$ m s^{-1} and $u_T = 0.102171$ m s^{-1} respectively.

APPLICATIONS: SAND VOLCANOES AND SHALLOW WATER FLOWS

The model predictions for this dynamic flow are difficult to validate with real geological field examples because observations generally refer to extinct sand volcanoes. For this reason, data describing the direct measurement of the flow rates during the homogeneous stage are not available. However, fountains of extruded sand–water mixtures have been observed to be up to 1·5 m high, for conduit dimensions in the order 0·05 m < r < 0·30 m and $H \sim 15$ m (Housner, 1958). The model presented in this paper provides the highest possible flow rates for a given set of boundary conditions. By equating the kinetic, $0.5\rho u^2$, and potential, $h\rho g$, energies of the fountain, it is possible to obtain the height of the fountain: $h = u^2/2g$, where the density of the mixture, ρ, cancels out.
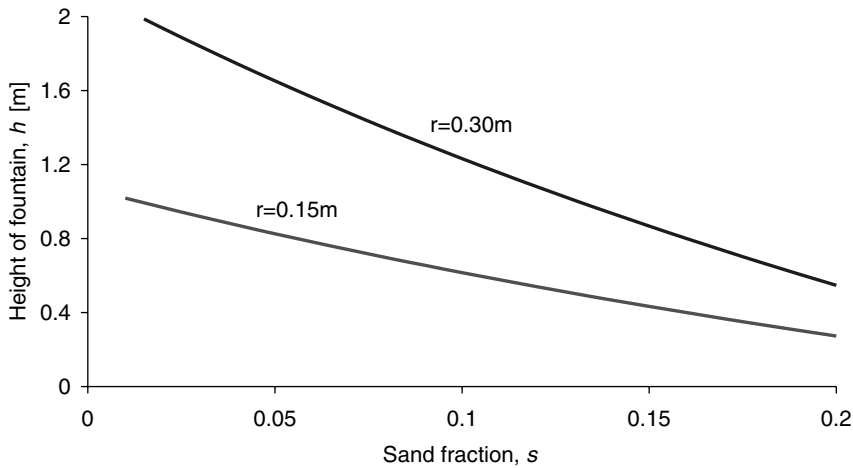
Figure 11 shows the height of the fountain, h, as predicted by the model. The length of the conduit is $H = 15$ m, and two example values were taken for the radius, $r = 0.15$ m and $r = 0.30$ m, and the maximum overpressure

$\Delta p = (\rho_L - \rho_W)gH = 73\,500$ Pa was considered as an indicator. Although these measurements are imprecise, they nevertheless suggest that the model predictions are consistent with the real phenomena. Moreover, the smooth cone features created during extrusion suggest low sand concentration in the erupted mixture, which supports the homogeneous flow assumption.
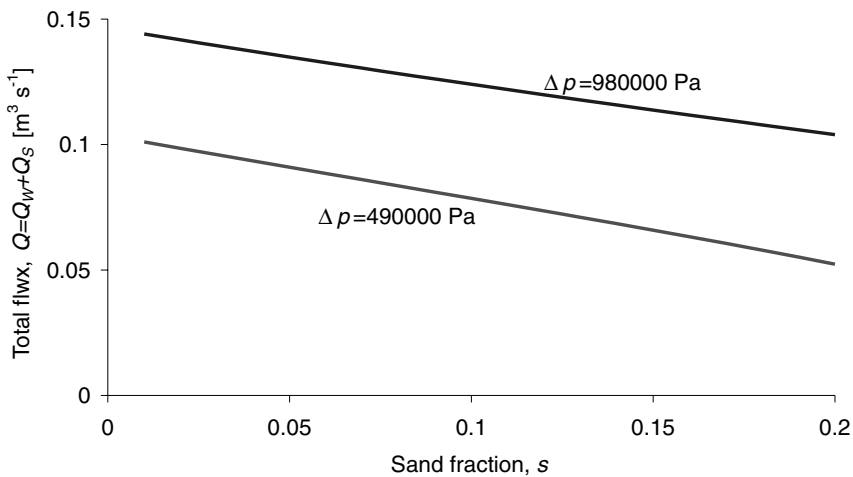
Fortunately, more precise empirical data are available to test the validity of the model from offshore drilling activities in deep water. In particular, in deep water in the Gulf of Mexico, there have been a number of oil fields in which drilling operations have intersected high-pressure layers of sand about 100 m below the sea floor. These young, poorly consolidated sediment layers have been observed to generate sand–water flows that ascend the well-bore and issue upwards as a jet onto the sea bed (Alberty *et al.*, 1997; Pelletier *et al.*, 1999; Alberty, 2000). The flows may persist for days or even weeks. The main difference from the natural analogue is the triggering mechanism: here, the drilling replaces the natural causes outlined in the Introduction, and the well bores seem to be generally longer than naturally occurring conduits, while the diameter of the well-bore is of the order of 0·1–0·5 m.

Video data collected by British Petroleum from remote submersible observations at the sea bed in the Gulf of Mexico suggest flow rates at the sea bed of order 0·01–0·15 m^3 s^{-1}, for conduit heights $H \sim 100$ m.

This observation is in accordance with the predictions of the model. Using the field observations of well bottom pressure and the dimensions

Fig. 11. The graph shows the height, as a function of sand fraction, of the fountain produced by a sand–water mixture extruded onto the surface. The overpressure is held constant, $\Delta p = 73\,500$ Pa, and the two curves represent two values of the estimated radius: $r = 0\cdot1$ m and $r = 0\cdot30$ m.

Fig. 12. Flow rate Q as a function of sand content s. The parameters used are: $H = 100$ m; $r = 0\cdot1$ m; $C_D = 0\cdot045$; and the overpressures, Δp, represent the maximum overpressures for average sediment densities $\rho_L = 1500$ kg m^{-3} and $\rho_L = 2000$ kg m^{-3} respectively. The values of the flux represent the maximum possible values; as the source is depleted, the value of the flux is expected to decrease. The predictions by the model are in accordance with the field observations, i.e. $Q \sim 0\cdot01$–$0\cdot15$ m^3 s^{-1}.

of the well-bore, it is possible to estimate the flow rate as a function of the sand content, and this is shown in Fig. 12. It is seen that, with a sand content in the range 0·1–0·2, the model replicates the estimates of flow rate on the sea bed. The parameters used are: $H = 100$ m; $r = 0\cdot1$ m, which corresponds to a typical diameter of 0·2 m; a typical friction factor for the rough walls of the conduit is $C_D = 0\cdot045$ (Moody, 1944); and the overpressures, $\Delta p = 490\,000$ Pa and $\Delta p = 980\,000$ Pa, represent the maximum overpressures for average sediment densities $\rho_L = 1500$ kg m^{-3} and $\rho_L = 2000$ kg m^{-3} respectively. The values of the flux represent the maximum possible values. During an eruption, the source is gradually depleted and the overpressure is dissipated, so the value of the flux will decrease. However, this comparison gives some support to our earlier predictions of vigorous sand–water flows at the sea bed for natural sand-volcano flows. Although the final deposits in sand

dikes may indicate much more sluggish flow, characteristic of the waning stage of the eruption, the intermediate flow may be much more vigorous. It is also positive that both the above sets of empirical data seem to be consistent with the model predictions within the limits of validity of the model as outlined in the assumptions.

EXTENSION TO PLANAR DIKES

Observations show that not all sand injections occur in the form of cylindrically shaped pipes. It was argued above that, when the sediments overlying the source bed are consolidated, the overpressure may create planar fractures, into which the sand is then injected. As most sand dikes that are now exposed at the surface were created in the geological past and uncovered only relatively recently by erosion of the surrounding sediments, it is very difficult to discern the

Fig. 13. Sand extrusions from planar dikes near the Pajaro River, Watsonville area, California. Furrows are spaced about 1·2 m apart (J. C. Tinsley, US Geological Survey).

properties of the flow that occurred within them at the time of injection. There are examples, however, where the details of the dike structures suggest that a low-density, fast flow may have taken place. In mainland Tierra del Fuego, Argentina, dikes exist in which there are large clasts with diameters of up to 0·25 m entrapped in a body of well-sorted, fine sand grains. Also, laminar flow surfaces parallel to the dike walls can be observed in the sand, and there is the presence of wall rip-ups. All these testify to rapid injection and a single-phase emplacement history (Winslow, 1983).

There are some, albeit rare, cases where sand has been observed to extrude directly from a planar dike. Examples include the Watsonville area of California, after the Loma Prieta earthquake of 1989 (Nakata *et al.*, 1999). Figure 13 shows sand extrusions from planar dikes near the Pajaro River, Watsonville area, California. Vertical dikes are also known to lead to the formation of large horizontal sills (Parize, 1988; Jolly & Lonergan, 2002). In certain circumstances, the latter could provide an escape route for the material flowing through the dike. Under these conditions, it is possible that a quasi-steady stage may develop similar to that assumed for the cylindrical conduits.

Although other vertical dikes may be arrested and may not lead to quasi-steady flow, the above field constraints suggest that it may be of interest to adapt the model developed for cylindrical conduits for a planar dike geometry. Figure 14 shows the idealized, steady extrusion of a sand–water mixture through a planar dike.
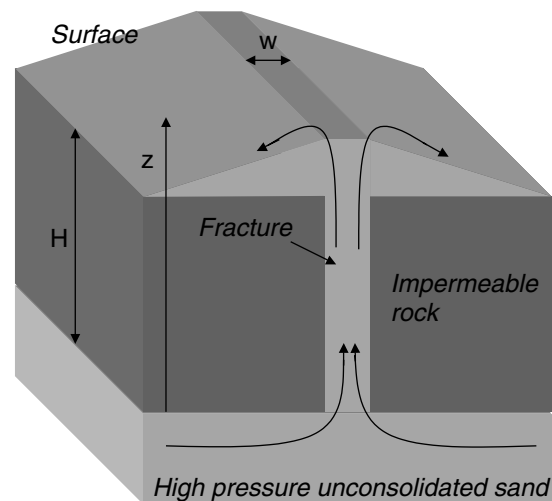
The model is adapted by replacing Eq. (2) with:

$$\frac{dp}{dz} = -\rho g - \frac{12\mu u}{w^2} - \frac{\rho C_D u^2}{w} \quad (15)$$
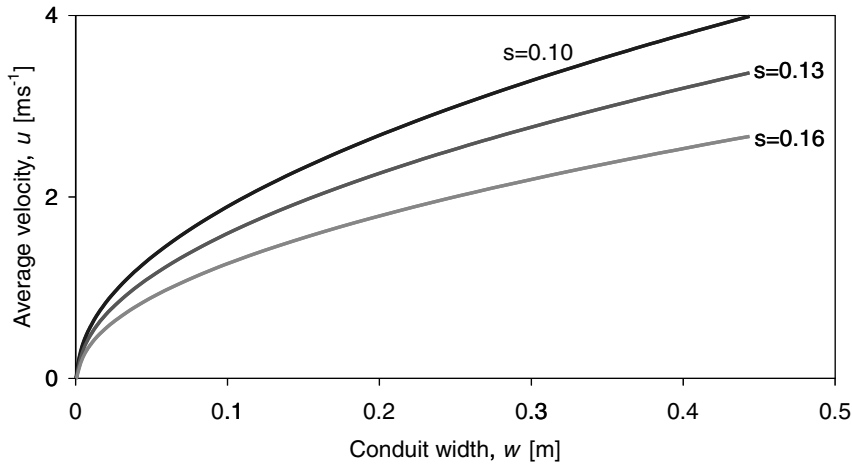
where w is the width of the fracture. The following equation replaces the previous expression for the average velocity: $u = (Q_W + Q_S)/w$, where Q_W and Q_S are now the volumetric fluxes per unit length of the dike and are measured in m^2 s^{-1}. This leads to the new upward velocity:

$$u = -\alpha + \sqrt{(\alpha^2 + \gamma)} \quad (16)$$

where $\alpha = \frac{6\mu}{\rho C_D w}$ represents the velocity for which

Fig. 14. The quasi-steady phase of a sand volcano eruption from a planar dike.

Fig. 15. Results from the model adapted for planar geometry. Parameters used: $H = 10$ m; $\Delta p = 35\ 000$ Pa; $C_D = 0.045$; the others are as usual.

the viscosity and the turbulent drag are comparable, and $\sqrt{\bar{\gamma}} = \sqrt{\frac{w}{\rho C_D}\left((\rho_w - \rho_s)sg + \frac{\Delta p}{H}\right)}$ denotes the flow speed in which the overpressure is balanced by the turbulent resistance alone. The qualitative properties of this solution are clearly analogous to Eq. (9); there are only quantitative differences in the flow rates as expected. Figure 15 shows some typical results.

As no data are available about the flows involved in the creation of dikes at greater depths ($H > 100$ m), this model cannot be directly validated. The sand concentrations may be higher than $s = 0.2$, or the mechanisms taking place may be different altogether from the one invoked here. Because of this, the model for the homogeneous flow remains only speculative in such domains. Further geological investigation should address this question. However, because of the relatively shallow nature of the process, the model is expected to be relevant for the extended extrusions observed after the Loma Prieta earthquake (Fig. 13).

CONCLUSION

Sand injections occur when a water-saturated sand bed is rapidly sealed by a low-permeability layer of mud. The general geometry of the sand injections depends on the behaviour of the host bed. Under certain circumstances, the sands can be forced to intrude the overlying layers but, in others, they may extrude on to the surface.

A model is proposed to describe the properties of a homogeneous and steady sand–water flow in a cylindrical conduit. The model is in accordance with field observations of sand extrusions from shallow sources (i.e. $H < 15$–20 m) leading to sand volcano eruptions producing fountains up to 5 m high, with flow rates of the order of 0.1–1.0 m^3 s^{-1} and sand concentrations of up to 20%. The numerical predictions are also found to match the data obtained from the analogous process of 'shallow water flows' induced by the deep-sea drilling of boreholes.

Field data suggest that the model of the flow in a cylindrical conduit is most appropriate for eruption through shallow unconsolidated sands. In deeper, more consolidated rocks, an overpressured sand may lead to fracturing of the host bed and to the formation of a dike. For completeness, the model can be extended to apply to a planar conduit geometry; similar controls on the flow rate and regimes as for the cylindrical case were found.

The analytical work presented here directly addresses only one of the various processes that may take place during sand injections. Work should be directed to the study of the initial propagation of the fracture/conduit and the rundown stage. Also, the model assumes homogeneous flow, and it would be interesting to extend this to other flow regimes.

for generously sharing their drilling data and video recordings of shallow water flows taken in the Gulf of Mexico from remote submersibles during drilling operations. We are also grateful to Dr Julio Friedmann and Dr Mads Huuse for their very helpful revisions of the paper.

NOMENCLATURE

C_D friction coefficient
d diameter of sand grains
g acceleration of gravity
H conduit height
p pressure
p_A atmospheric pressure
Q total flux
Q_S sand flux
Q_W water flux
r radius of conduit
Re Reynolds' number
s sand fraction
s_C sand fraction at which effective viscosity goes to infinity
u average velocity of sand–water mixture
u_S sand velocity
u_T terminal velocity of sand grains
u_W water velocity
w width of fracture
z height along the conduit
Δp overpressure
μ effective viscosity
μ_0 water viscosity
ρ average density of sand–water mixture
ρ_L average density of overlying sediments
ρ_S density of sand
ρ_W density of water

REFERENCES

Alberty, M. (2000) Shallow water flows: a problem solved or a problem emerging. Paper OTC 11971. *OTC Annual Technical Conference and Exhibition*, Houston, TX, May 1–4.

Alberty, M., Hafle, M., Minge, J. and Byrd, T. (1997) Mechanism of shallow waterflows and drilling practices for intervention. Paper OTC 8301. *OTC Annual Technical Conference and Exhibition*, Houston, TX, May 5–8.

Boehm, A. and Moore, J.C. (2002) Fluidized sandstone intrusions as an indicator of paleostress orientation, Santa Cruz, California. *Geofluids*, **2**, 147–161.

Borrello, A.V. (1962) Sobre los Diques Claticos de Tierra del Fuego. *Extr. Rev. Mus. Plata (Nueva Serie) Secc. Geol.*, **5**, 155–191.

Cosgrove, J.W. (2001) Hydraulic fracturing during the formation and deformation of a basin: a factor in the dewatering of low-permeability sediments. *AAPG Bull.*, **85**, 737–748.

Cross, W. (1893) Intrusive sandstone dikes in Granite. *Bull. Geol Soc. Am.*, **5**, 225–230.

Diller, J.S. (1889) Sandstone dikes. *Bull. Geol Soc. Am.*, **1**, 411–442.

Dixon, R.J., Schofield, K., Anderton, R., Reynolds, A.D., Alexander, R.W.S., Williams, M.C. and Davies, K.G. (1995) Sandstone diapirism and clastic intrusion in the Tertiary submarine fans of the Bruce-Beryl Embayment, Quadrant 9, UKCS. In: *Characterization of Deep Marine Clastic Systems* (Eds A.J. Hartley and D.J. Prosser), *Geol. Soc. London Spec. Publ.*, **94**, 77–94.

Galli, P. (2000) New empirical relationships between magnitude and distance for liquefaction. *Tectonophysics*, **324**, 169–187.

Gill, W.D. and Kuenen, P.H. (1957) Sand volcanoes on slumps in the Carboniferous of County Clare, Ireland. *Q. J. Geol. Soc. London*, **113**, 441–460.

Housner, G.W. (1958) The mechanism of sandblows. *Bull. Seismol. Soc. Am.*, **48**, 155–161.

Huang, Q. (1988) Geometry and tectonic significance of Albian sedimentary dykes in the Sisteron area, SE France. *J. Struct. Geom.*, **10**, 453–462.

Jolly, R.J.H. and Lonergan, L. (2002) Mechanisms and controls on the formation of sand intrusions. *J. Geol. Soc. London*, **159**, 605–617.

Lonergan, L., Lee, N., Johnson, H.D., Cartwright, J.A. and Jolly, R.J.H. (2000) Remobilization and Injection in Deep-water Depositional Systems: Implications for Reservoir Architecture and Prediction. *GCSSEPM Foundation 20th Annual Research Conference Deep-Water Reservoirs of the World*, Houston, TX, pp. 515–532.

Marsh, B.D. (1981) On the crystallinity, probability of occurrence, and rheology of lava and magma. *Contrib. Mineral. Petrol.*, **78**, 85–98.

Moody, L.F. (1944) Friction factors for pipe flow. *Trans. Am. Soc. Mech. Eng.*, **66**, 671–684.

Nakata, J.K., Meyer, C.E., Wilshire, H.G., Tinsley, J.C., Updegrove, W.S., Peterson, D.M., Ellen, S.D., Haugerud, R.A., McLaughlin, R.J., Fisher, G.R. and Diggles, M.F. (1999) The October 17, 1989, Loma Prieta, California, earthquake – selected photographs. Digital Data Series DDS-29. US Department of the Interior, US Geological Survey. Online publication: http://wrgis.wr.usgs.gov/dds/dds-29/

Neumann-Mahlkau, P. (1976) Recent sand volcanoes in the sand of a dike under construction. *Sedimentology*, **23**, 421–425.

Newson, J.F. (1903) Clastic dikes. *Bull. Geol Soc. Am.*, **14**, 227–268.

Nichols, R.J. (1995) The liquification and remobilisation of sandy sediments. In: *Characterization of Deep Marine Clastic Systems* (Eds A.J. Hartley and D.J. Prosser), *Geol. Soc. London Spec. Publ.*, 94, 63–76.

Nichols, R.J., Sparks, R.S.J. and Wilson, J.N. (1994) Experimental studies in the fluidization of layered sediments and the formation of fluid escape structures. *Sedimentology*, **41**, 233–253.

Obermeier, S.F. (1996) Use of liquefaction-induced features for paleoseismic analysis – an overview of how seismic liquefaction features can be distinguished from other features and how their regional distribution and properties of source sediment can be used to infer the location and strength of Holocene paleo-earthquakes. *Eng. Geol.*, **44**, 1–76.

Obermeier, S.F. (1998) Liquefaction evidence for strong earthquakes of Holocene and latest Pleistocene ages in the states of Indiana and Illinois, USA. *Eng. Geol.*, **50,** 227–254.

Parize, O. (1988) Sills et diques greseux sedimentaires; paleomorphologie, fracturation precoce, injection et compaction (Sills and dikes of sedimentary sandstone; paleomorphology, fracturing, injection and compaction). PhD Thesis, Ecole Nationale Superieure des Mines de Paris, 313 pp.

Pelletier, J.R., Ostermeier, R.M., Winker, C.D., Nicholson, J.W. and **Rambow, F.H.** (1999) Shallow water flow sands in the deepwater Gulf of Mexico, some recent Shell experience. *1999 International Shallow Water Flow Forum*, Folke EngelMark, October 6–8.

Seed, H.B. (1979) Soil liquefaction and cyclic mobility evaluation for level ground during earthquakes. *J. GeoTech. Eng., Am. Soc. Civil Eng.*, **94,** 1055–1122.

Strachan, L.J. (2002) Slump-initiated and controlled syndepositional sandstone remobilization: an example from the Namurian of County Clare, Ireland. *Sedimentology*, **49,** 25–41.

Takahama, N., Otsuka, T. and **Brahmantyo, B.** (2000) A new phenomenon in ancient liquefaction – the draw-in process, its final stage. *Sed. Geol.*, **135,** 157–165.

Truswell, J.F. (1972) Sandstone sheets and related intrusions from Coffee Bay, Transkei, South Africa. *J. Sed. Petrol.*, **42,** 578–583.

Wallis, G.B. (1969) *One-Dimensional Two-Phase Flow*, 1st edn. McGraw-Hill, New York. 408 pp.

Walsh, T.J., Combellick, R.A. and **Black, G.L.** (1995) *Liquefaction Features from a Subduction Earthquake; Preserved Examples from the 1964 Alaska Earthquake.* Report of Investigations 32. Washington Division of Geology and Earth Resources, Olympia, WA, USA. 80 pp.

Waterson, C.D., (1950) Note on the sandstone injections of Eathie Haven, Cromarty. *Geol. Mag.*, **87,** 133–139.

Winslow, M.A. (1983) Clastic dike swarms and the structural evolution of the foreland fold and thrust belt of the southern Andes. *Geol. Soc. Am. Bull.*, **94,** 1073–1080.